

Structures at Meso- and Micro-scales in the Sutlej section of the Higher Himalayan Shear Zone in Himalaya

SOUMYAJIT MUKHERJEE – soumyajitm@gmail.com (Department of Earth Sciences, Indian Institute of Technology Bombay, Mumbai, India)

ABSTRACT: Study of structural geology of the Higher Himalayan Shear Zone (HHSZ) in the Sutlej section reveals S-C fabric, mineral fish, syntectonic growth of porphyroblasts, stretching of clasts, crenulation cleavages, intrafolial folds, duplexes, boudins, and micro-scale hat-shaped minerals and rare sedimentary textures. In migmatites, the S-C fabrics are defined by various thicknesses of leucosomes and melanosomes of various curvatures. In micro-scale, either mineral fish or aligned undeformed grains characterize S-fabrics. Porphyroblasts were either stretched or nucleated syntectonically during the extensional shearing. Hat shaped minerals indicate brittle shear. Intrafolial folds are of various thicknesses and some of their axial traces parallel the shear planes. In the two detachments within the HHSZ, the dominant ductile shear sense is top-to-NE, elsewhere the sense is exclusively top-to-SW. The brittle shear sense in the HHSZ is also top-to-SW. While the brittle shearing postdated the migmatization event in the HHSZ, boudinage was presumably a syn-migmatization process.

KEYWORDS: Higher Himalayan Shear Zone, ductile deformation, brittle deformation, micro-structure.

1. INTRODUCTION

The Higher Himalayan Shear Zone (HHSZ)- a longitudinal strip of the Himalaya- consists of greenschist to amphibolite facies rocks. The HHSZ has been a subject of intense research for its structural and tectonic uniqueness (reviews in Godin et al., 2006; Yin, 2006; Mukherjee, 2007; Mukherjee & Koyi, in press, 1; 2). The HHSZ is bound by the Main Central Thrust (MCT) at south and the South Tibetan Detachment System-Upper (STDS_U) at north (Godin et al., 2006). The former thrust shows a top-to-SW sense of shearing and the later detachment a prominent top-to-NE and a relict top-to-SW shearing (Yin, 2006 and references therein). In different sections of the Himalaya, the average timing of this SW shearing has been ~ 25 Ma with a much younger pulse ~ 3.3 Ma, whereas the NE shearing took place ~ 18 Ma (Johnson and Harley, 2003; Godin et al., 2006 and references therein). A second extensional shear zone- the South Tibetan Detachment System-Lower (STDS_L)- has been noted in some sections of the HHSZ (see Godin et al., 2006 for review). In their field studies, Mukherjee & Koyi (in press, 1) traced both the STDS_U and the STDS_L in the Sutlej section of the HHSZ (Fig. 1) based solely on the shear sense and not on the basis of the morphology of these indicators. Further, as the tectonic boundaries were traced only on the river section on the basis of small-scale ductile shear sense indicators, it was impossible to locate them at distance, nor using a binocular. They traced these tectonic units as straight lines for the sake of presentation in the terrain where structural observations can conveniently be made only along the road section. A number of other geological studies are also available from the HHSZ in this section (e.g. Singh, 1993; Vannay and Grasemann, 1998; Grasemann et al., 1999; Vannay et al., 2004). In this work, a detail photographic description of structures from the HHSZ, Sutlej section is presented.

From the lower part of the HHSZ in the Sutlej section, up to the VT, the peak metamorphism is characterized by an increase in temperature from 610 to 700°C and drop in pressure from 900 to 700 MPa (Vannay et al., 1999). Northward from the VT, the temperature increases from 570 to 750°C at nearly constant pressure of 8 MPa. These thermo-barometric data, along with the presence of the staurolite zone at the base- and profound melt activities at the top of the HHSZ indicate inverted metamorphism within it (Vannay and Grasemann, 2001). Reviewing the P-T

data of this terrain, Vannay and Grasemann (2001) concluded that: (i) the peak metamorphism of the HHSZ was achieved at 30 km depth; and (ii) the P-T evolution of the terrain matches with the geochronologic constraints suggesting that the HHSZ was exhumed by simultaneous thrusting of the MCT-zone and extensional shearing of (two strands of?) the STDS.

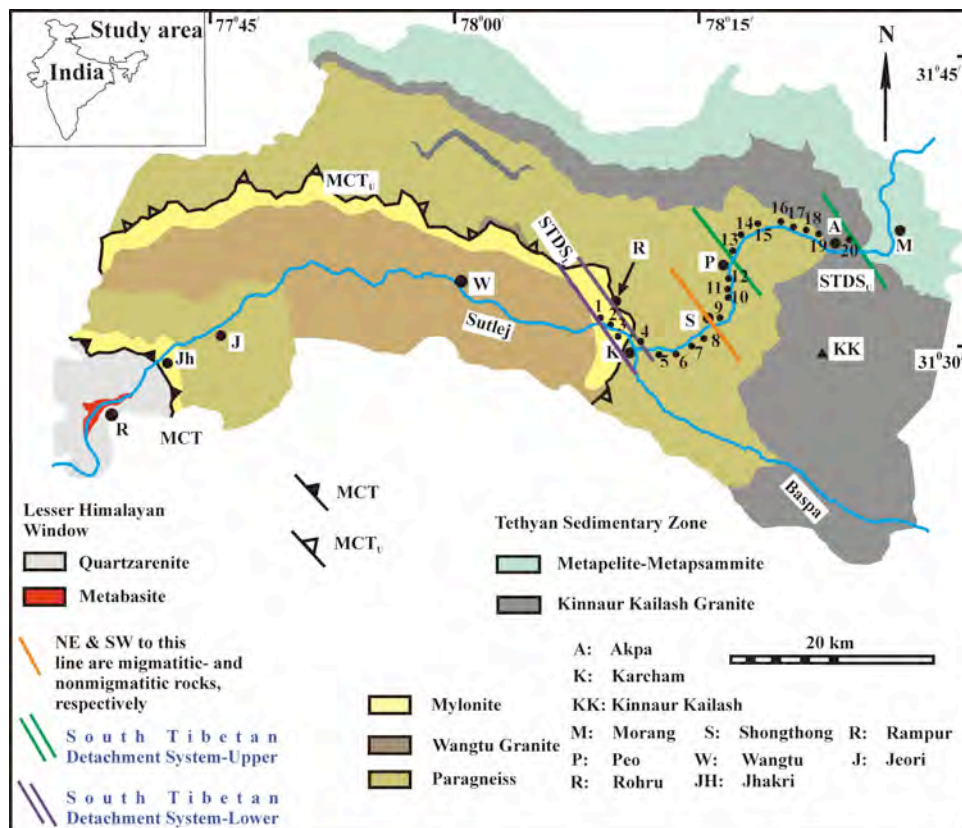


Figure 1 – Geological map of the Higher Himalayan Shear Zone (compiled and simplified from Singh, 1993; Srikantia & Bhargava, 1998; and Vannay & Grasemann, 1998). The location of the Main Central Thrust (MCT) is as per Singh (1993). Srikantia and Bhargava's (1998) Vaikrita Thrust is denoted by Godin et al.'s (2006) 'MCT-Upper' (MCT_U). The two strands of the extensional ductile shear zone-- the STDS_L and the STDS_U are shown. Numbers 1 to 20 represent sample locations.

2. STRUCTURES AND TEXTURES

2.1. S-C Fabric

The S-fabrics (Berthé et al. 1979) indicate shearing along the primary shear C-planes. The shear strain is most intense at the contacts between the S- and the C-fabrics. Equidistant from a pair of C-planes, the S-fabrics attains minimum curvature where the shear strain is minimum. The S-fabrics show progressively increasing curvature towards the C-planes and at their contact they are tangent to the latter. At few places the S-planes also behaved in a brittle manner and seem to be inseparable from the brittle P-planes (Figs. 3c, 4b). In different ways, the S-fabric is manifested- in meso-scale: 1. alternate layers of thick leucosomes and thin and close spaced melanosomes define the S-fabric (Figs. 2b, 5a). 2. The C-plane may be defined by thick leucosome layers (Figs. 3a, 4a, 4d). 3. Close spaced melanosomes can define the S-planes (Fig. 2a). 4. Sigmoid bulge of leucosomes define the S-fabric (Figs. 2c, 2d, 5d). 5. Asymmetric, rather irregular-shaped quartz veins can define the S-fabric (Figs. 3d, 5b). 6. Thick bulge of

melanosomes define the S-fabric (Fig. 5c). 7. Near symmetric bulges of leucosomes are ambiguous shear sense indicators (Fig. 3b). 8. The C-plane may sharply truncate the S-planes as found in migmatites (Fig. 4c). 9. Adjacent layers of leucosomes can be differentially affected by synthetic secondary shearing (Fig. 5a). In micro-scale the following variability of S-C fabrics were noted. 1. As S shaped sigmoidal or Z-shaped zigmoidal fabric; 2. tilted almost undeformed mineral grains (Figs. 6a, b); 3. a single curved deformed mineral grain defining the S-fabric (Fig. 7b), 4. a number of mineral grains of different orientation that define the S-fabric (Fig. 7c). The C-plane may be defined by elongated minerals, by a number of undeformed, usually very fine grained minerals, or by rather thick zones of recrystallization. Since leucosomes were found to define both the S- and the C-planes in meso-scale, the migmatization event was essentially a syntectonic process (e.g. Marchildon & Brown, 2003; Misra et al., 2009).

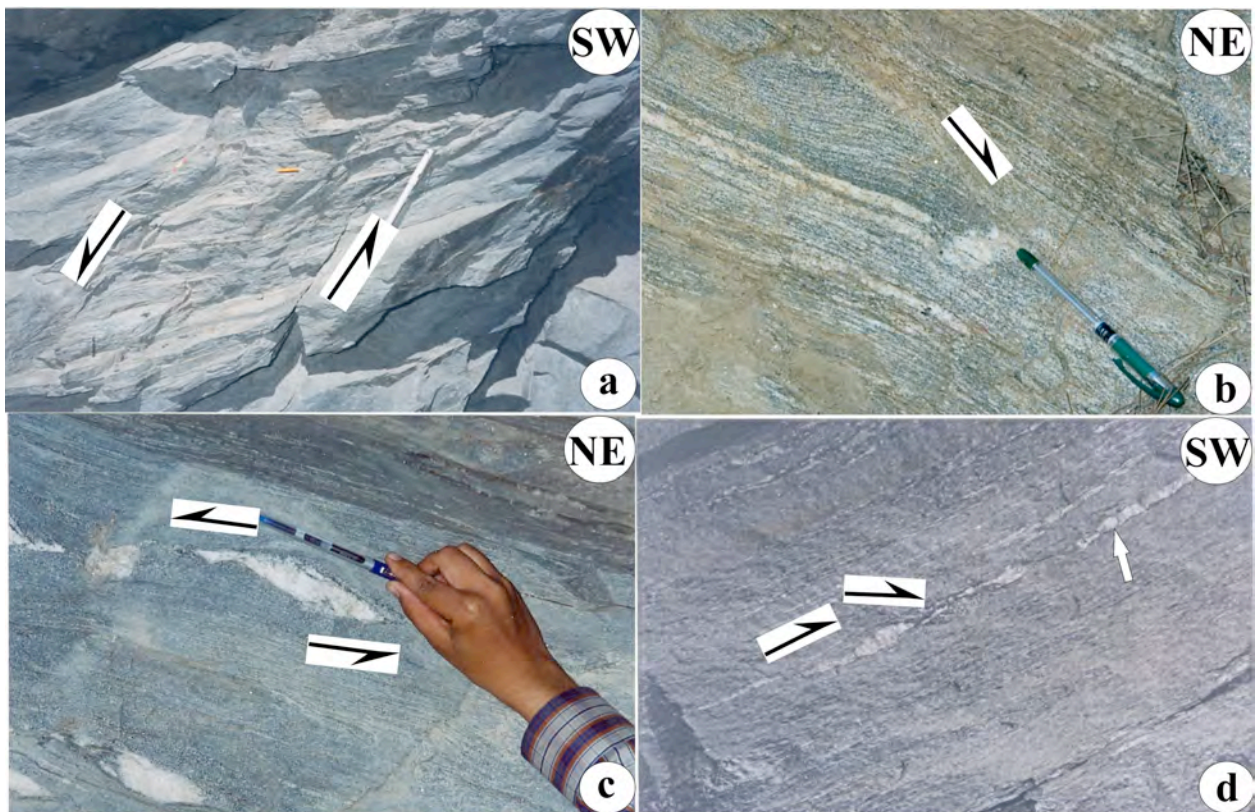


Figure 2a – Sharp sigmoid (or zigmoid- to be more specific) lines define the S-fabric. Non-migmatitic rock. Location: 5. 2b – Dense thin innumerable layers of melanosomes (arrow) and few thick leucosomes are sigmoidally bent. The C-plane is not a tangent, but sharply cuts the S-planes. Migmatite. Location: 9. 2c – Within dense layers of melanosomes, neary sigmoid (or zigmoid- to be more specific) leucosome defines an S-fabric. Migmatite. Location: 16. 2d – At very low angle to the melanosome layer, sigmoid leucosomes give the shear sense. The C-plane is occupied by leucosome (full arrow). Migmatite. Location: 13.

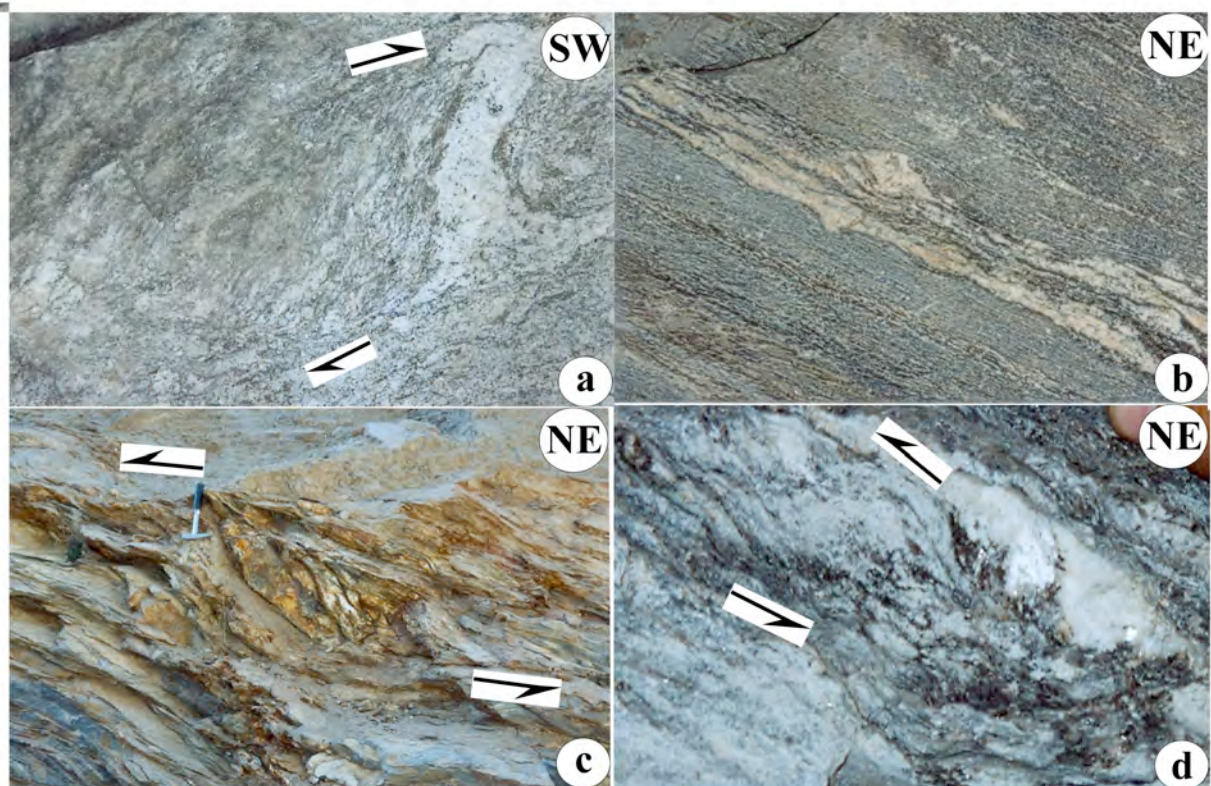


Figure 3a – A thick layer of leucosome and several thin layers of leucosomes and melanosomes define the S-fabric. Migmatite. Location: 9. 3b – Leucosomes are parallel to the migmatitic foliation. Weak asymmetry precludes determination of the shear sense. Migmatite. Location: 10. 3c – S-C fabric in schistose rock (or Z-C fabric, to be more specific) but has later developed brittle deformation along the same planes. Migmatite. Location: 18. 3d – Thick leucosome and thin melanosome layers define sigmoid S-fabric (or zigmoid Z-fabric, to be more specific). Migmatite. Location: 19.

2.2. Mineral Fish

These are lozenge-shaped porphyroclasts and single crystals in fine-grained matrices in mylonitized rocks (ten Grotenhuis et al. 2002; Mukherjee, in press). Mineral fish (Figs. 6c-d, 7a-c, 8a-b, 10b) are special types of S-C fabric that are the most common ductile shear sense indicators in micro-scale. Mineral fish are most commonly defined by micas ('mica fish' of Lister & Snoke, 1984). Rarely garnet is also crystal plastically deformed into a characteristic fish shape (Fig. 10b). The C-planes are straight, envelopes the mineral fish and are defined by very fine-grained recrystallized minerals. Sigmoid-shaped fabrics show progressive curving near the bounding C-planes. Either these three shapes are defined by single minerals (Figs. 6c-d, 7a-b, 8a-b, 10b) or as aggregate of minerals (Fig. 7c) that are usually micas. The cleavages of mineral fish are tilted to the primary shear plane in a synthetic fashion. In some cases rigid quartzofeldspathic minerals are wrapped by incompetent mica grains that defines the fish geometry (Fig. 6d). Both sigmoid- (Figs. 6d, 7b-c, 8a, 10b) and parallelogram-shaped (Figs. 6c, 7a, 8b) mineral fish were encountered. The two tips of the sigmoid fish sometimes show different amount of curvature (Fig. 7b). Rather irregular grain margins of parallelogram mineral fish are seldom encountered (Fig. 8b).

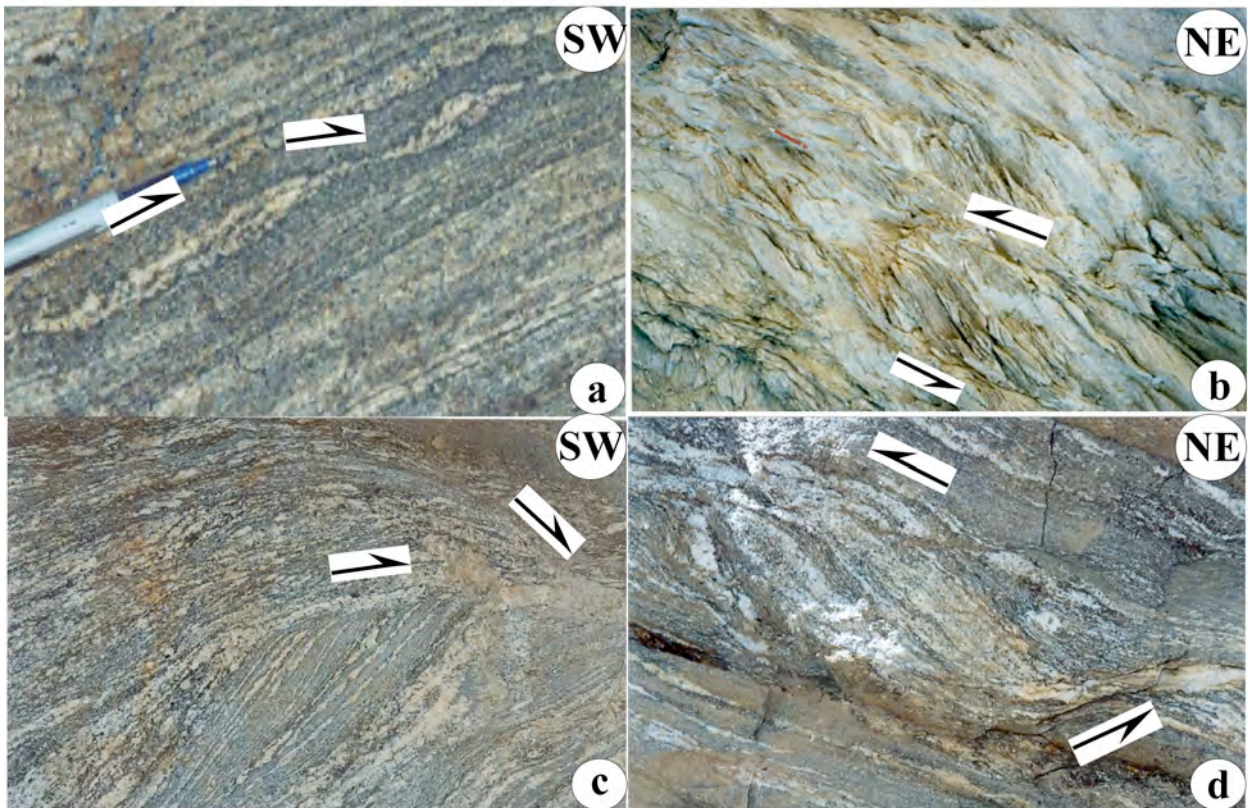


Figure 4a – Sigmoid leucosome layers interconnected with tails that underwent Synthetic secondary shearing. Migmatite. Location: 12. 4b – Close-spaced straight S-fabric (or Z-fabric, to be more specific) that are curved only near the C-plane. Migmatite. Location: 13. 4c – Numerous thin melanosome layers and few thick leucosome layers that act as S-fabric are cut by C-the plane. The C-plane is defined by thick layers of leucosomes. The leucosomes vary thin thickness along their lengths. Location: 14. 4d – Thick leucosomes define the S fabric (or the Z-fabric, to be more specific). Brittle secondary shear plane developed. Migmatite. Location: 15.

Extensive migration of boundary of grains from matrix into fish might lead to modification of fish shape almost beyond recognition. Inclusion of alkali feldspar inside sigmoid mica fish are also noted (Fig. 8a). Such more competent inclusions were found to be undeformed. Extensively recrystallized minerals in the matrix define the S-fabric of Bèrthe et al. (1979). The studied mineral fish do not possess any notch or mouth at their corners. Pressure solution might be a reason of sigmoidality of some of the fish (e.g. Bell and Cuff 1989). In some cases, mica fish are found to be completely surrounded by quartzofeldspathic minerals (Figs. 7a-b, 8b) and lack any tail. The shear sense in those cases were specified by tracing the C-plane orientation known from the same thin-section outside the field of view.

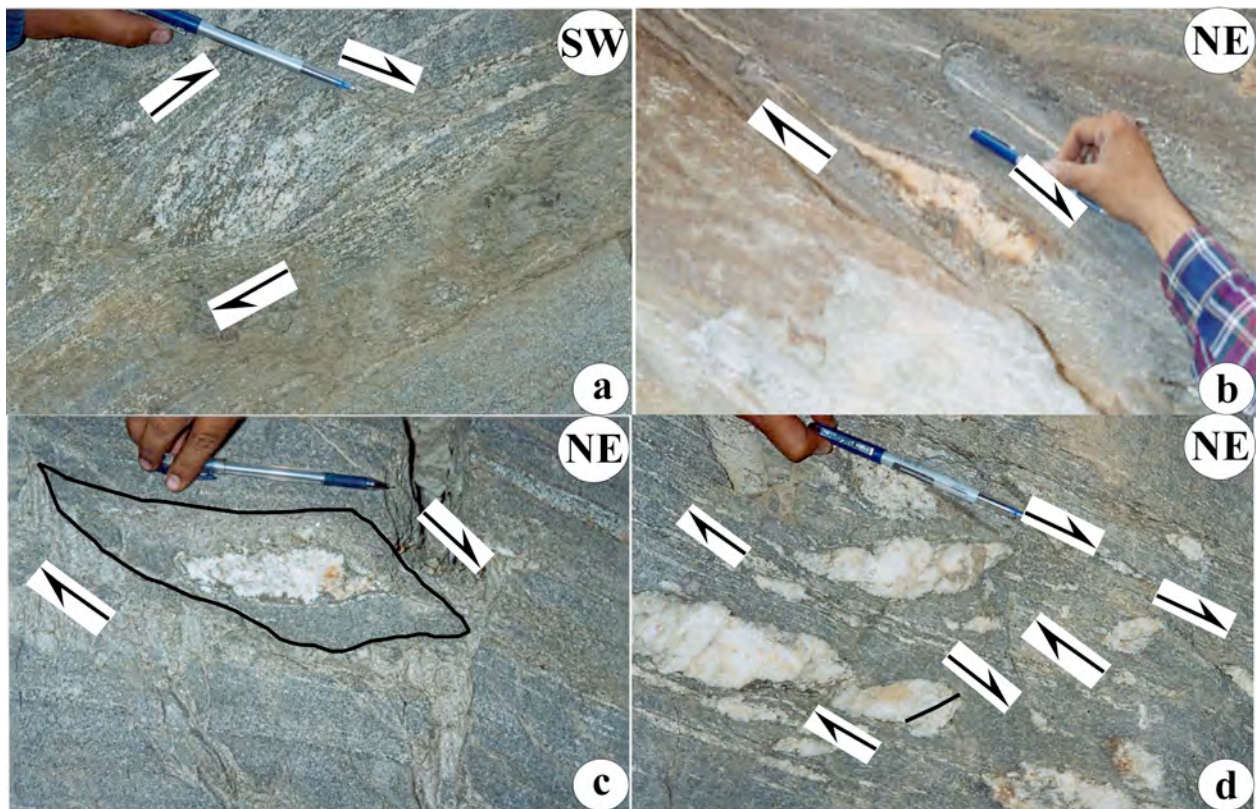


Figure 5a – A number of thick leucosomes and numerous thin melanosomes define the S-fabric. Synthetic shearing lowers the local orientation of the S-fabric. Migmatite. Location: 16. 5b – Asymmetric quartz vein acts as the S-fabric. Long tail indicates pronounced shearing. The quartz vein is also pinched along the main foliation. Migmatite. Location: 17. 5c – A sigmoid bulge of leucosome inside another sigmoid bulge of melanosome. Leucosome. Location: 18. 5d – S-fabric defined by leucosomes of various shape. A rootless intrafolial fold also shows the same shear sense. The sigmoid bulges vary in sizes but each of them consists of a few thin melanosome layers. Migmatite. Location: 19.

2.5. Other structures

As observed in micro-scales (Mukherjee & Koyi, 2009), flanking structures were sometimes observed in field-scales (Figs. 18b, -c) where prominent drag folds near the cross-cutting element were usually decipherable but only rarely the exact slip sense (Fig. 15d). In few rare cases, crenulation cleavages were observed in separated mica aggregates. Post-tectonic biotite grains were found to cut across the crenulated micas (Fig. 8c). Near Karcham area, garnet grains are porphyroblastic and show a wide variety of deformation features under microscope. These are: 1. extreme elongation parallel to the foliation plane or a flattening perpendicular to those planes (Figs. 9a, 10a); 2. intrafolial folding with axial plane and the limbs dipping SW (Fig. 9d); 3. Brittle V –pull apart structure (Hipperitt, 1993) indicating a top-to-SW sense of shearing (Fig. 9c). The V-opening may be curved and filled up with (recrystallized) quartzofeldspathic minerals; 4. Inclusions of quartz (S-internal) parallel to the foliation plane (S-external) (Fig. 9a); 5. Sigmoid inclusion pattern (Vernon, 2004 and references therein), a top-to-NE sense of shearing and syntectonic growth of the porphyroblast (Fig. 10c); 6. Pressure shadow defined by micas as the boundaries and flattened quartzofeldspathic minerals as its contents (Fig. 10d); and 7. Rather uncommon are garnet fish that are affected by both primary and the secondary shearing

(Fig. 10b). The secondary shearing is an indication of a component of pure shear in the deformed rocks (Cottle et al., 2007 and references therein).

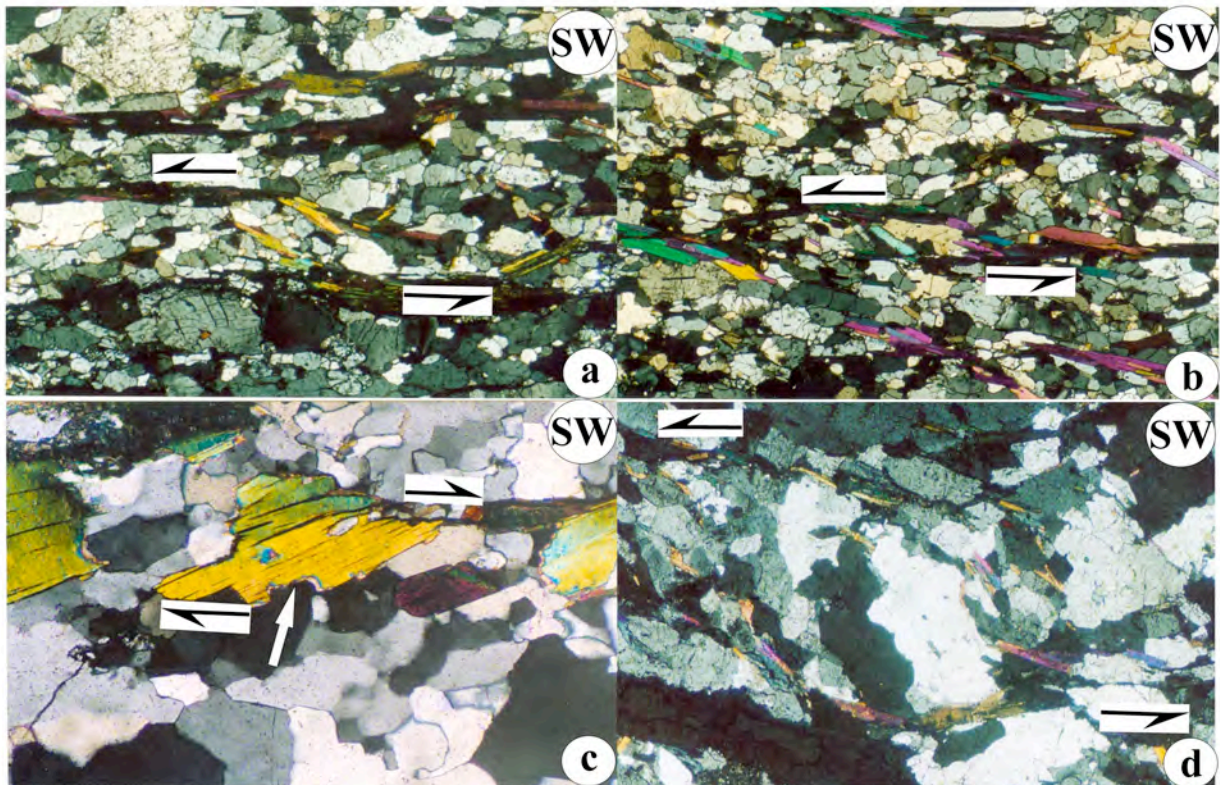


Figure 6a – Isolated grains of mica defines S fabric (or the Z-fabric). Quartzofeldspathic minerals are not elongated and do not define the S fabric. Aggregates of micas define the C-planes. Sample location: 5. 6b – The S- and the C-planes are defined by micas in such a way that a parallelogram shape is produced. Quartzofeldspathic minerals are not elongated and do not define the S fabric. Sample location: 6. 6c – A parallelogram-shaped muscovite fish. The C-plane is defined by preferred orientation of micas only at one of its corners. At the other side, quartzofeldspathic minerals migrated towards the fish (full arrow). Non-migmatite. Sample location: 7. 6d – Thin individual micas define an ‘S’ sigmoid (or ‘Z’ zigmoid) and bound feldspar grains. Non-migmatite. Sample location: 8.

Sedimentary texture is also displayed about 300 m near to Karcham near an unnamed bridge. Subrounded quartzofeldspathic grains with inter-grain calcite (Fig. 11a) resembles a sedimentary fabric that has survived a low strain. In other places, extensive migration of alkali feldspar grains towards less competent mica grains were abundantly documented (Fig. 11b-c). The migrated boundaries of these grains are either rectangular or triangular. Late stage brittle faults cut across quartz, feldspar as well as foliation micas (Figs. 11d). Due to a lack of suitable marker minerals across the fault planes, the brittle slip sense was not always decipherable.

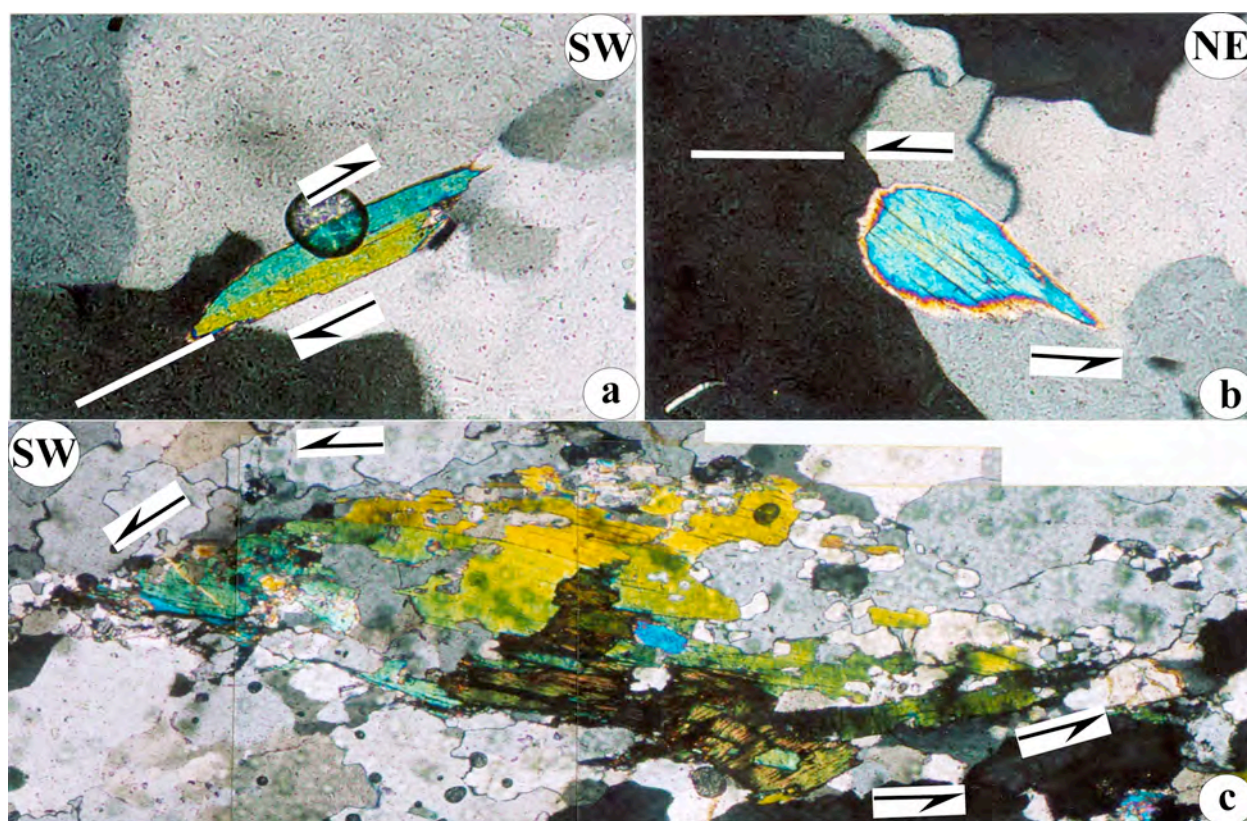


Figure 7a, b – An isolated parallelogram-shaped mica fish (Fig. 7a) and a nearly sigmoid mica fish (Fig. 7b) noted at a very high magnification. No adjacent fish trail is present. The orientation of the primary shear plane is extrapolated (white line) from elsewhere in the thin-section. Sample location: 9. 7c – A zigmoid muscovite fish that has undergone extensively recrystallization and matrix feldspar grains migrated into it. Curved cleavages of the fish are still decipherable that reliably gives the shear sense. Sample location: 10.

Brittle slip in micro-scale is demonstrated by trapezoid-shaped minerals- most commonly micas- from the entire HHSZ (Figs. 12a-d; also see Mukherjee & Koyi, in press, 1, 2 for more examples). The longest arms of these hat-shaped minerals dip northeasterly and represent slip of the hat towards SW (Fig. 12a). The brittle shear sense matches with the standard duplexes documented in field studies. The other arms of the trapezoid grains are also straight indicating that grain boundary migration did not shape them. Where slipped and transported to a relatively longer distance, these hat minerals are completely surrounded by quartzofeldspathic minerals (Fig. 12c). One hat may override the other in a symmetric fashion. However, symmetric hats do not decipher any shear sense (Fig. 12b-c). Hats of different minerals and minor variation of shapes have also been described in Mukherjee (2007), Mukherjee (2008), Mukherjee & Koyi (in press, 1; in press, 2).

Intrafolial folds (as discussed in Ghosh, 1993) are developed throughout the Sutlej section of the HHSZ. Inside the two strands of the detachment (STDS_U and the STDS_L), their limbs and axial planes dip towards southwest and demonstrate a top-to-NE shear sense. Elsewhere in the HHSZ, the limbs and the axial planes of these folds dip towards northeast and represent a top-to-SW shear sense. The limbs of these folds may not be of equal thickness (e.g. Figs. 13a, c, 14a-b, 16b, 17a-b). Inside the migmatitic terrain, thicker leucosome layers more prominently show these folds. In the same trains of intrafolial folds, the style and geometry (amplitude, wavelength,

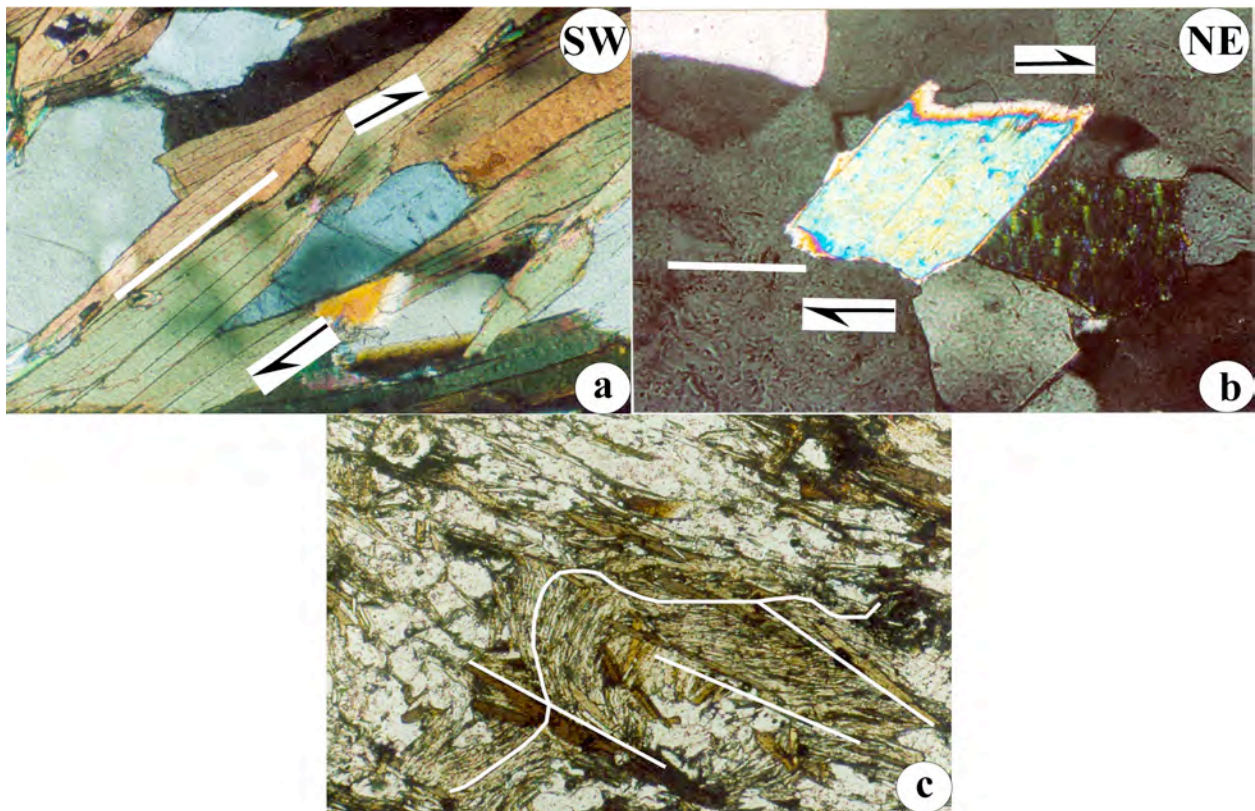


Figure 8a – An alkali feldspar fish nucleated over a number of muscovite grains. A tail has formed at one of the sides but not at the other. This indicates differential effects of pulling at the corners of the same grain. Grain margins of the host minerals efficiently acted as C-shear planes. Sample location: 11. 8b – An isolated parallelogram-shaped mica fish at a very high magnification. No adjacent fish trail is present. The orientation of the primary shear plane is extrapolated (white line) from elsewhere in the thin-section. Sample location: 1. 8c – Late phase long thin biotite grains transpose over locally persistent round hinge folded foliation of muscovite. Curvature of the folded foliation must not be confused with the S-fabric. Sample location: 2.

curvature of the hinge point etc.) of individual folds show remarkable variation (Fig. 15c). Their hinge zones may be thicker than the limbs. Tracing intrafolial folds along a train one may encounter a box fold (Fig. 15c). No regional folds exist in the study area as revealed by uniformly dipping foliation planes (Fig. 14d). This in turn indicates that the studied intrafolial folds are certainly not parasitic to any large fold, hence are reliable shear sense indicators. Extreme shearing can lead to three possibilities on the intrafolial folds. These are: 1. Breakage of the limbs leading to mutually separated rootless intrafolial folds (Figs. 14b, 16c). 2. The axial trace becomes sub-parallel to the shear plane so that the exact shear sense is ambiguous to decipher (Figs. 14c, 15a, 15b). 3. Along the limb brittle faulting takes place leading to opposite sense of curvature of the foliation planes across these faults (Figs. 13d, 15d).

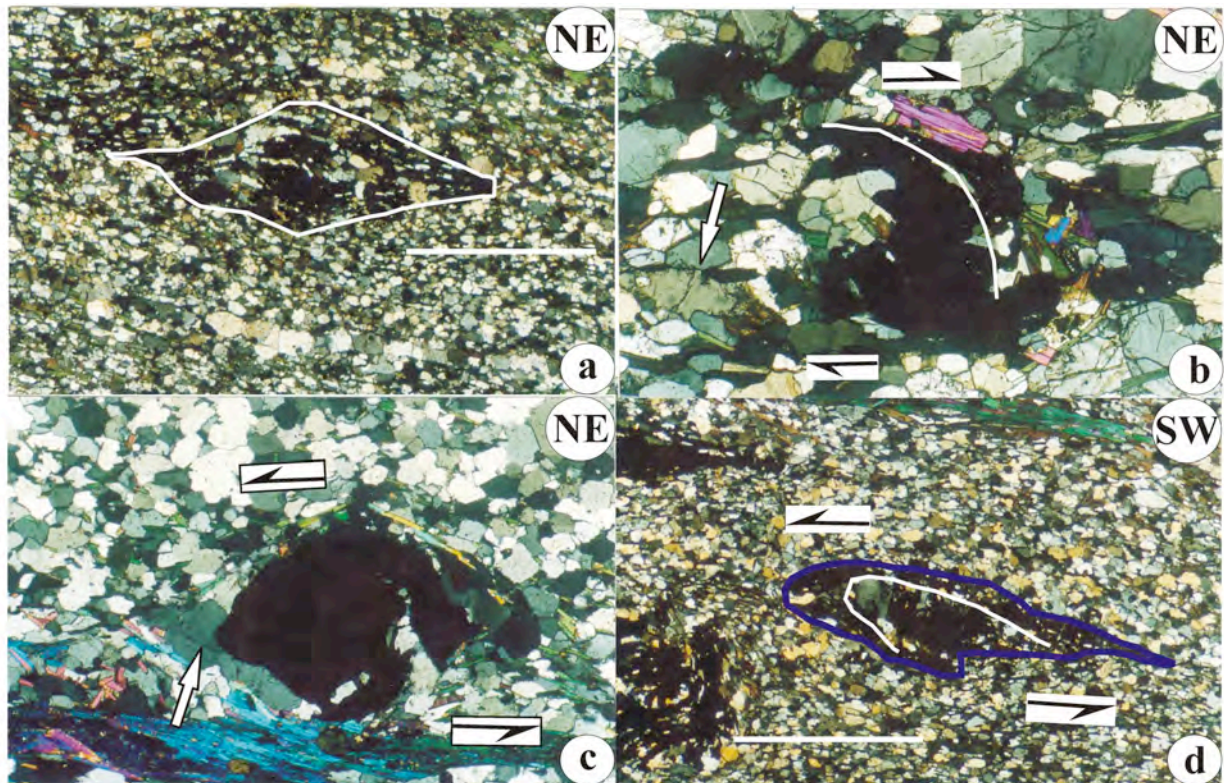


Figure 9a – Lenticular porphyroblastic garnet fish with trend of inclusions of feldspar matching with that of the external foliation. Therefore the garnet nucleated synkinematically. Trend of the external foliation is shown with a white rectangle. Non-migmatitic rock. Sample location: 3. 9b – Synkinematic nucleated porphyroblastic garnet grain showing curved inclusion pattern that is discordant with the external foliation. Undeformed straight boundaries of quartzofeldspathic grains in the matrix as well as those of micas define the external foliation (full arrow). Matrix minerals extensively migrated towards the grain from two directions. Sample location: 4. 9c – A V-pull apart of porphyroblastic garnet that indicates the brittle shear sense. At opposite corners of the grain, recrystallization of matrix minerals took place and gave rise to larger grains (arrow). Passive folds of foliation towards the V-opening is noticed. Sample location: 1. 9d – A sheared asymmetric somewhat irregular shaped porphyroblastic garnet containing inclusions that are discordant with the external foliation (white straight line) and is intrafolially folded (white curve). Sample location: 3.

Random networks of leucosomes unaffected by ductile shearing in migmatitic rocks (Fig. 18a) possibly indicate that the granitic melt crisscrossed the parent rock after the ductile shearing event. At other places in the migmatite, brittle fault planes were observed where SiO_2 -rich melt occupied the fault planes (Fig. 18b-c). No leucosome or melanosome layers could be identified as markers across the fault plane, therefore the sense of slip remained indeterminate.

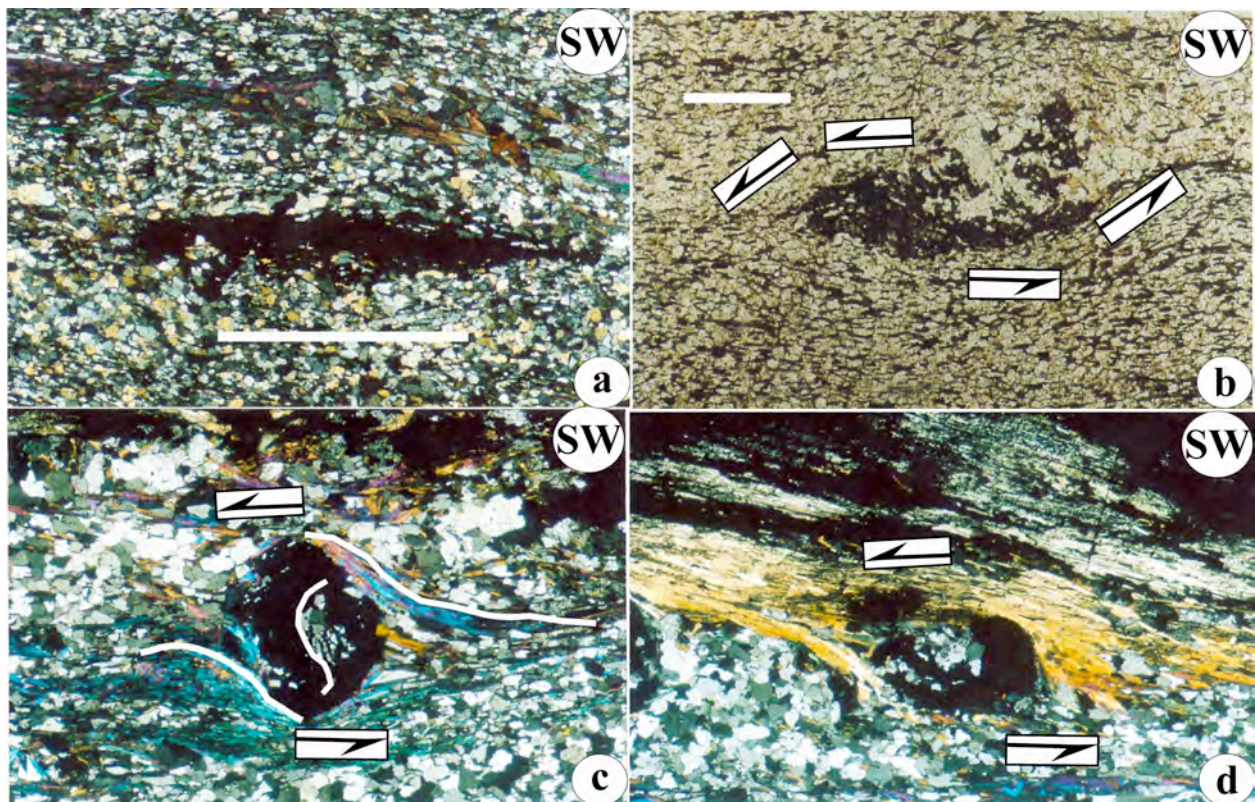


Figure 10a – Parallel to the foliation plane (white line) the porphyroblastic garnet grain underwent extreme stretching. Non-migmatitic rocks. Sample location: 2. 10b – A sigmoid garnet porphyroblast fish with long tail at one side. Thin short discrete biotite grains in the matrix define the primary shear plane. Sample location: 4. 10c – A porphyroblastic syntectonically nucleated garnet with its center showing sigmoid inclusion pattern. Matrix foliation wraps around the grain similar to a delta structure. Sample location: 3. 10d – A sigma-structure of garnet that prominently displays the sense of shearing. At the two opposite corners, tapering zones of pressure shadow is prominently displayed. Sample location: 2.

A phase of local brittle-ductile extension parallel to the main foliation was deciphered throughout the HHSZ based on boudins of diverse morphologies. At few places, the tectonic force was insufficient to completely separate potential boudins (Figs. 19a, -c). Boudinage by shearing along southwesterly dipping planes, possibly produced simultaneous and synthetic to the top-to-SW brittle shearing, is also evident at a number of places (Figs. 19b-d). Similarly secondary shearing synthetic to the top-to-SW ductile shearing also led to interconnected boudins (Fig. 20d). The inter-boudin space of low strain is marked by accumulation of granitic melts (Fig. 19b). This indicates that boudinage took place probably during the migmatization event (Marchildon and Brown, 2003; Misra et al., 2009). Very rarely, the leucosome layers are themselves boudinaged into interconnected lenticular bulges (Fig. 20a). The melanosomes defining the main foliation are curved towards the inter boudin space defining spectacular necking / scar folding/ pinching / infolding/ passive folding (Figs. 20d, 21).

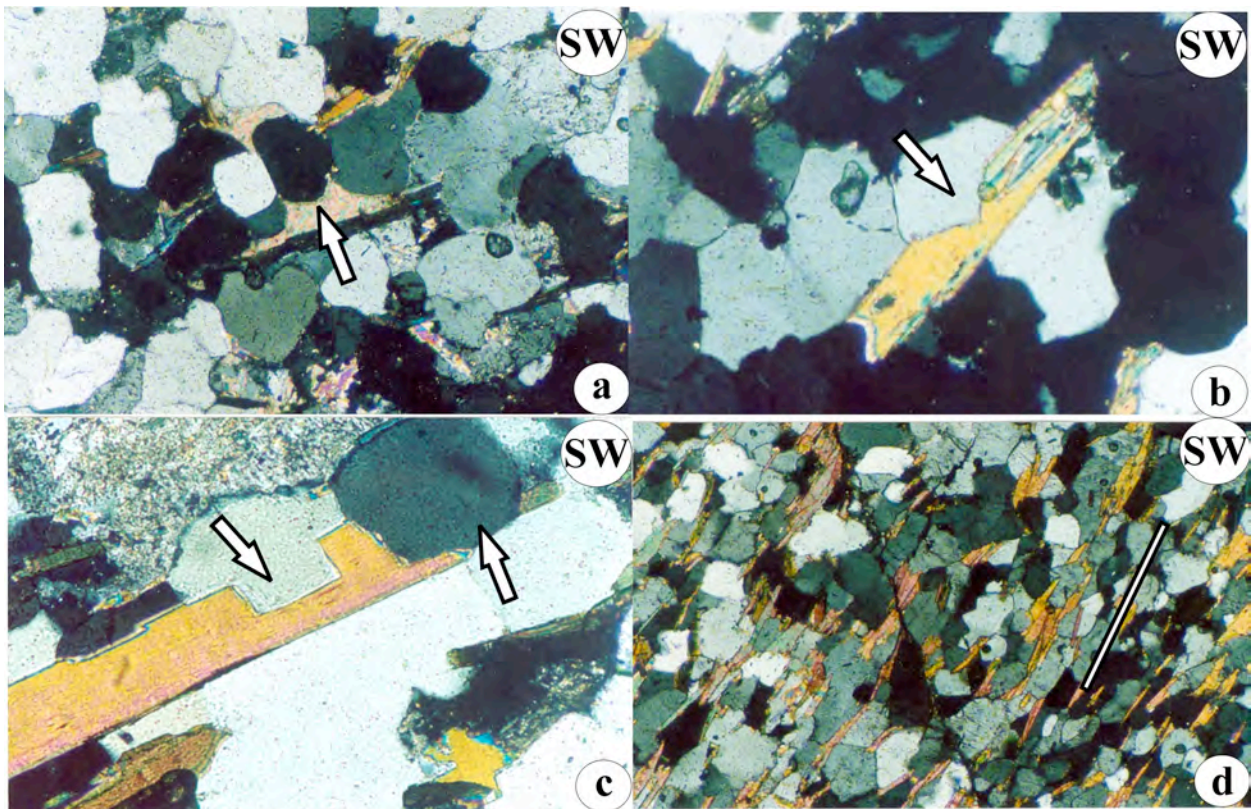


Figure 11a – The arrow shows calcite between alkali feldspar grains. The texture resembles a sedimentary rock. Non-migmatitic rock. Sample location: 5. 11b,c – Arrows show migration of alkali feldspar grains from the matrix towards the less competent micas. Sample number: 8. 11d – A brittle fracture at a high angle to the foliation plane (white line). Non-migmatitic rock. Sample location: 6.

Duplexes (e.g. McClay & Insley, 1986) with widely different dimensions but a uniform top-to-SW shear sense are observed in field-studies in the HHSZ (Figs. 22-24). Interestingly, the ductile primary shear planes coincide with the brittle shear plane indicating that the former planes reactivated during the brittle shear planes to give rise to duplexes. The brittle shear P-planes dip towards NE and are inclined at the Y-planes (See Passchier & Trouw, 2005 for brittle plane terminologies). The P-planes are more curved and are tangential at the boundaries of the Y-planes. Geometrically therefore, the S-C fabric is similar to the P-Y fabric. Synthetic Riedel-planes (R') are sometimes developed along with the P-Y fabrics but are less ubiquitous in the HHSZ. In some exceptional cases, a single bulge of rock defining the P-plane was observed (Fig. 24). No granitic melts were found to accumulate in either the P- or the Y-planes (Figs. 22-24). This indicates that the duplex movement postdates the migmatization event. Where R' -planes developed and no Y-planes, the P-planes are also well formed. The R' -P structures of brittle deformation resemble the S-C' fabric of the ductile regime. Figure 25 presents a structural summary of the Sutlej section of the HHSZ.

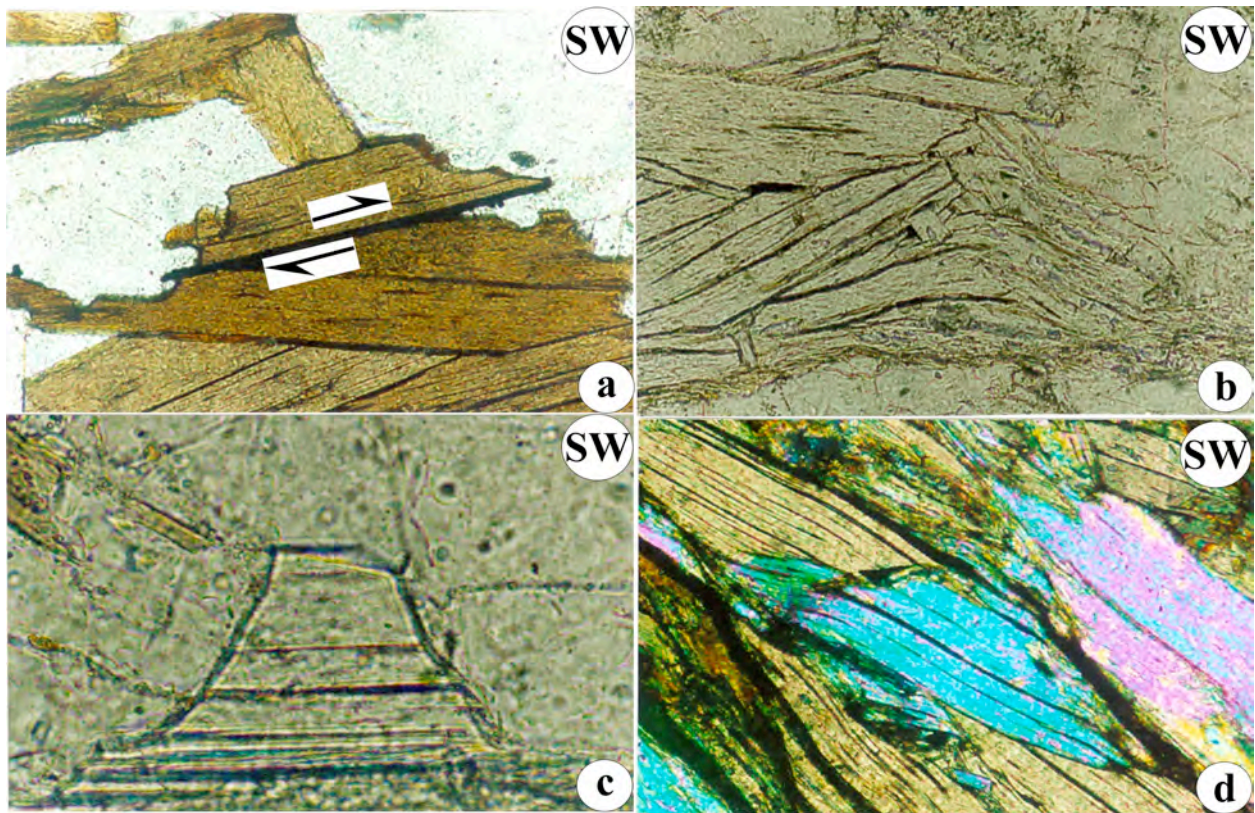


Figure 12a – Trapezoid shaped biotite overrides a number of other biotite grains. Migmatitic rock. Sample location: 18. 12b,c – Symmetric stack of muscovite grains that do not reveal any brittle sense of shearing. Migmatitic rock. Sample location: 9. 12d – A trapezoid shaped inclusion of muscovite grain within a muscovite host grain. Does this indicate any movement sense of the included grain? Non-migmatitic rock. Sample location: 12.

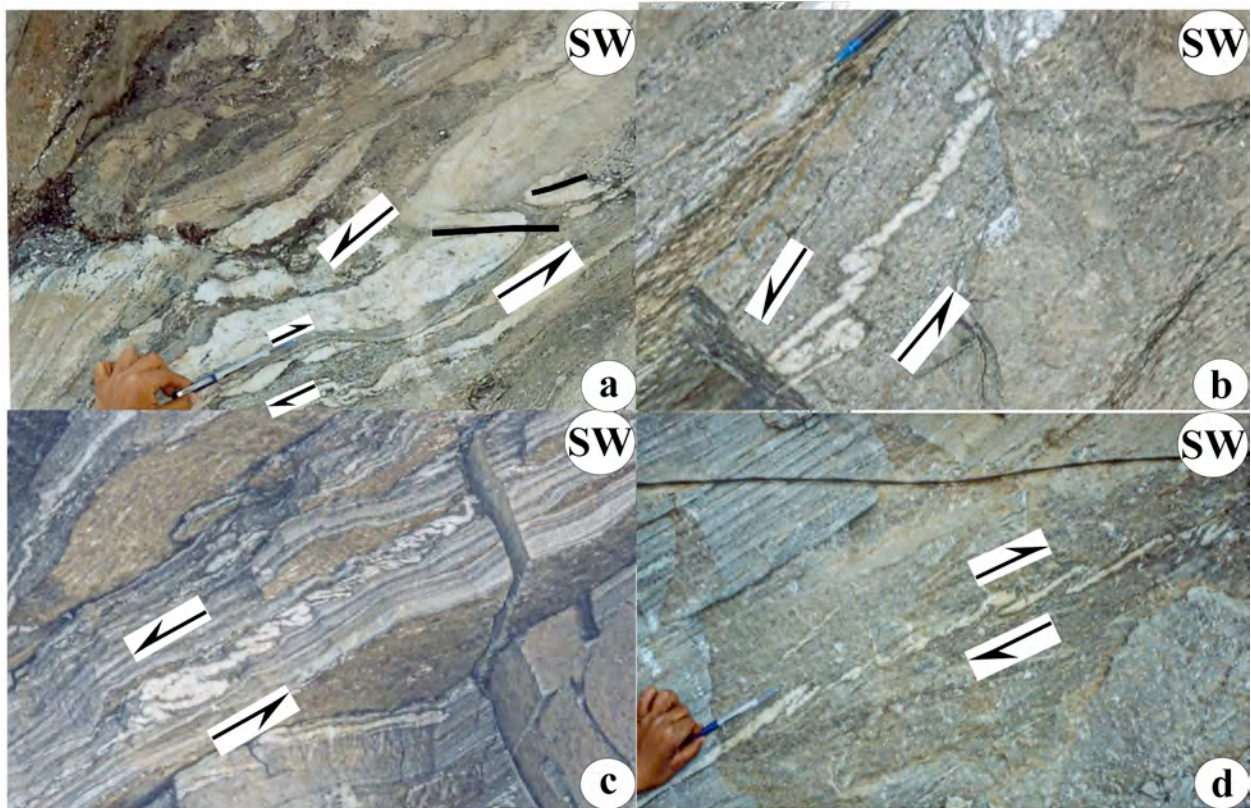


Figure 13 – Migmatitic gneiss. 13a – Thick quartz layer folded with its axial traces and limbs dipping in the same direction. Intense shearing disrupted a part of the layer into a rootless fold. Location: 6. 13b,c – Shear strain presumably varied in the shear zone so that rootless folds are not everywhere developed. Intrafolial folds vary in amplitude in a train. Location: 8. 13d – A different manifestation of intense shearing is found in a train of intrafolial folds: a set of limbs are disrupted. Location: 17.

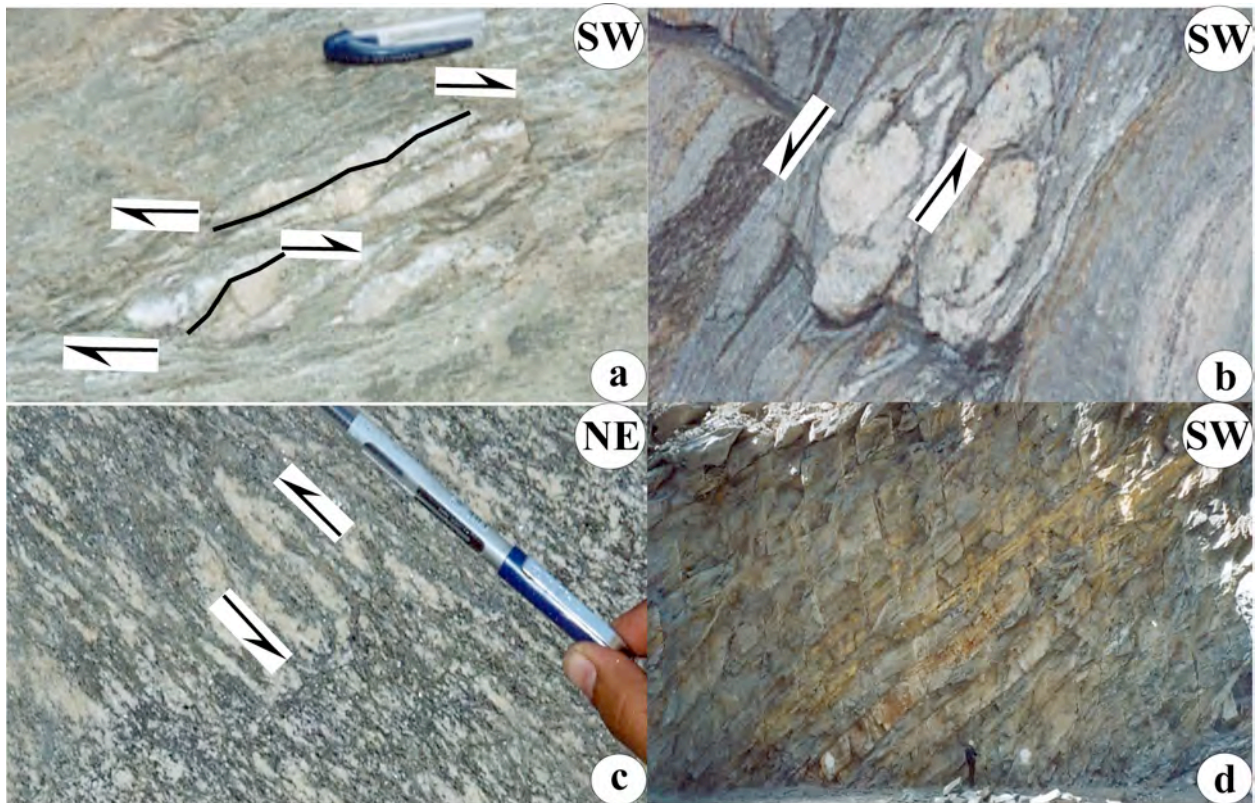


Figure 14a – Centimeter scale intrafolial folds with sharper fold hinges reveal the same sense of shear. Migmatitic rock. Location: 9. 14b – Intrafolial fold with very thick and rounded hinge area. Migmatitic rock. Location: 9. 14c – Ductile shearing has been so intense that the axial traces are sub-parallel to the main foliation and the folds assumed a hook shape. The shear sense has been assigned from other fabrics near this outcrop. Migmatitic rock. Location: 12. 14d – Where the intrafolial folds and other shear sense indicators are observed, they are accompanied by a remarkable straight and long main foliation planes over long distance. This indicates that the intrafolial folds are not parts of any major folds. Non-migmatitic rock. Location: 3. Geologist Sujoy Kanti Ghosh as marker.

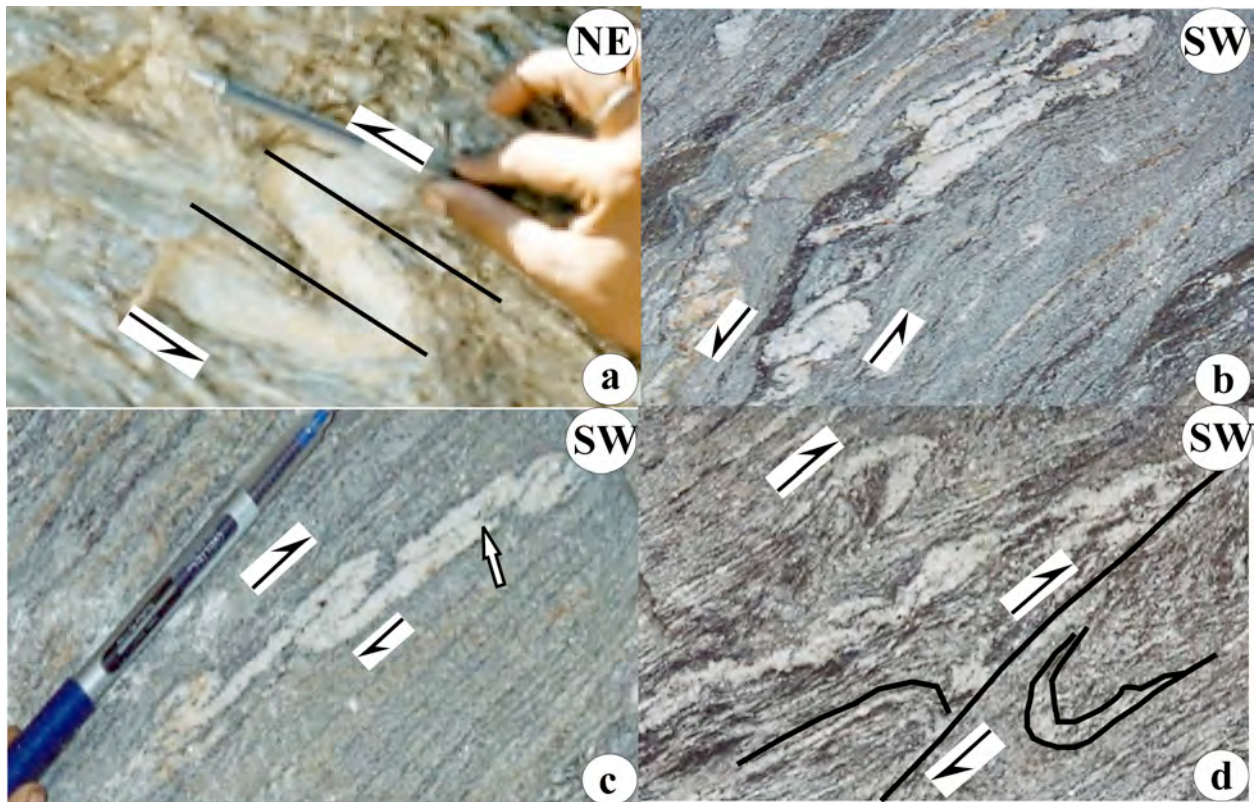


Figure 15a – Intense ductile shearing made axial trace of the intrafolial fold sub-parallel to the primary shear plane. Migmatitic rock. Location: 11. 15b – Intrafolial folds in a train with a set of limbs much thinner than the other set. Across the main foliation, these folds reveal variation in tightness, interlimb angle and amplitude. Migmatitic rock. Location: 14. 15c – Along the same train of intrafolial folds, many irregular features are observed (full arrow). Intense shearing at places disrupted intrafolial folds along main foliation in a brittle manner. Migmatitic rock. Location: 13. 15d – Intense shearing at places disrupted intrafolial folds along main foliation in a brittle manner. Migmatitic rock. Location: 15.

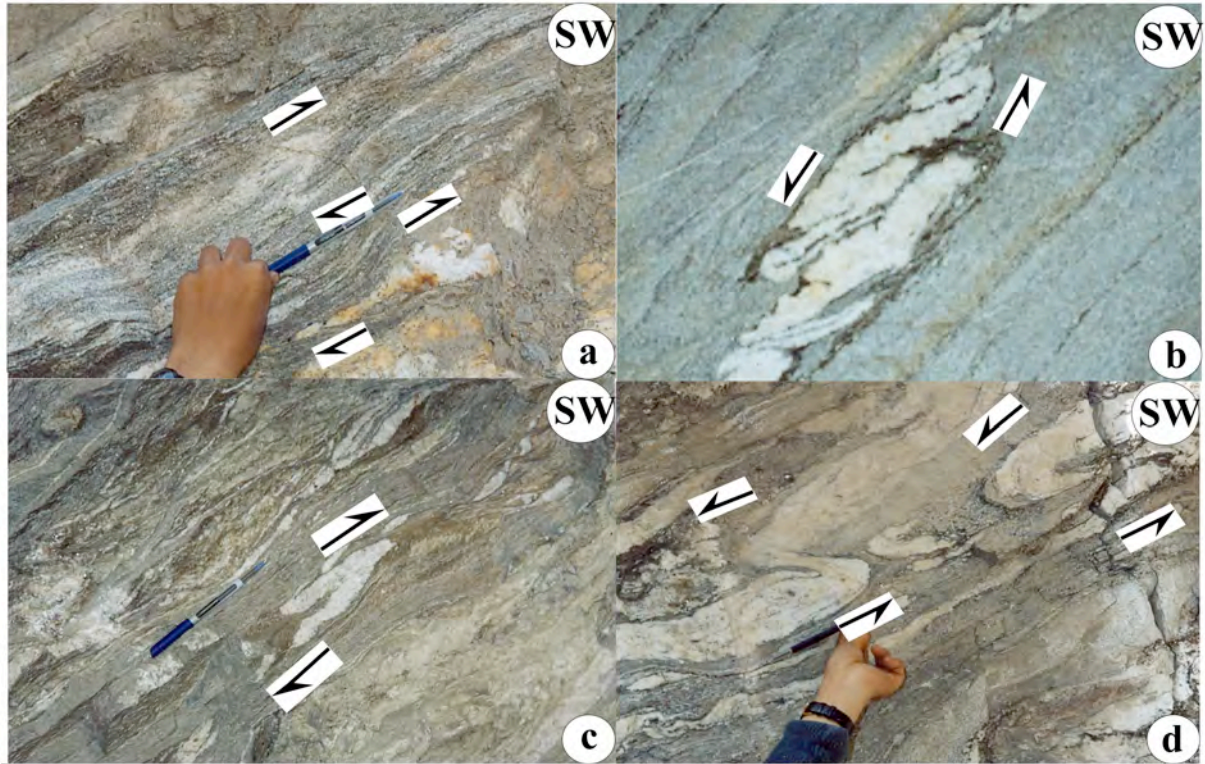


Figure 16a – Intrafolial folds with thick hinge, thin limbs of different thickness; one of the folds is sharply truncated by the shear plane. Migmatitic rock. Location: 3. 16b – Overturned fold with straight hinge area sharply cut and enveloped by the C-plane. Non-migmatitic rock. Location: 3. 16c – Overturned flame fold of quartz vein. Intense shearing led to near parallelism between the axial trace and the shear plane. Shear sense is deciphered from other fabrics near the fold. Non-migmatitic rock. Location: 3. 16d – The shear plane behaved ductilely to brittle ductilely so that in some cases the intrafolial folds are disrupted along sharp planes. Non-migmatitic rock. Location: 3.

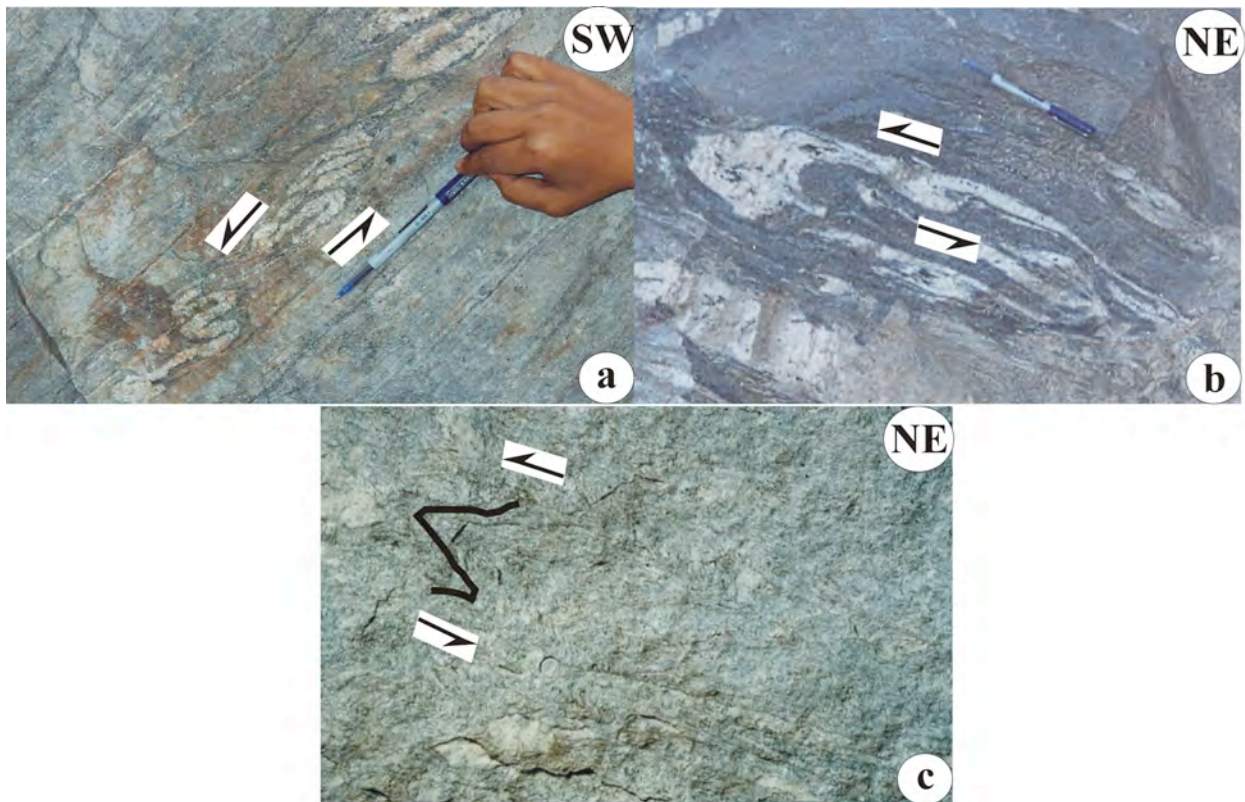


Figure 17a – Intense shearing led to S-shaped (or hook shaped) intrafolial folds of quartz veins with axial traces sub-parallel to the C-shear planes. Non-migmatitic rock. Location: 3. 17b – Distinct layers of leucosomes and melanosomes folded into round hinged overturned fold. Migmatitic rock. Location: 3. 17c – Faint kink fold of foliation planes indicate the same sense of shearing as those given by adjacent shear fabrics not in the photo. Non-migmatitic rock. Location: 5.

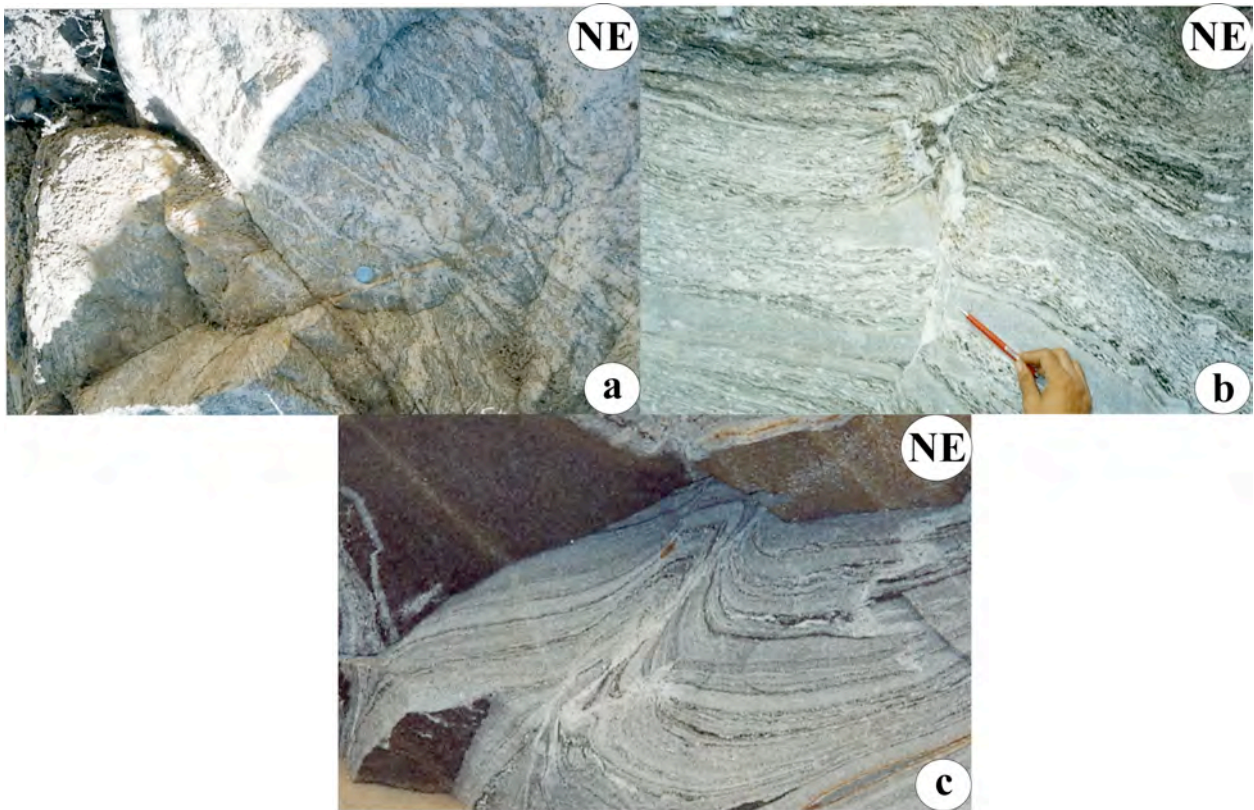


Figure 18a – Irregular network of leucosomes. Not indicative of any shear sense. Migmatitic rock. Location: 10.
18b, c – Flanking structures: thick irregular quartz rich layer acts as the cross-cutting element and migmatitic foliation defined by alternating thin layers of leucosomes and melanosomes define the host fabric elements. No host fabric acts as a distinct marker. Migmatite. Locations: 14, 15, respectively.

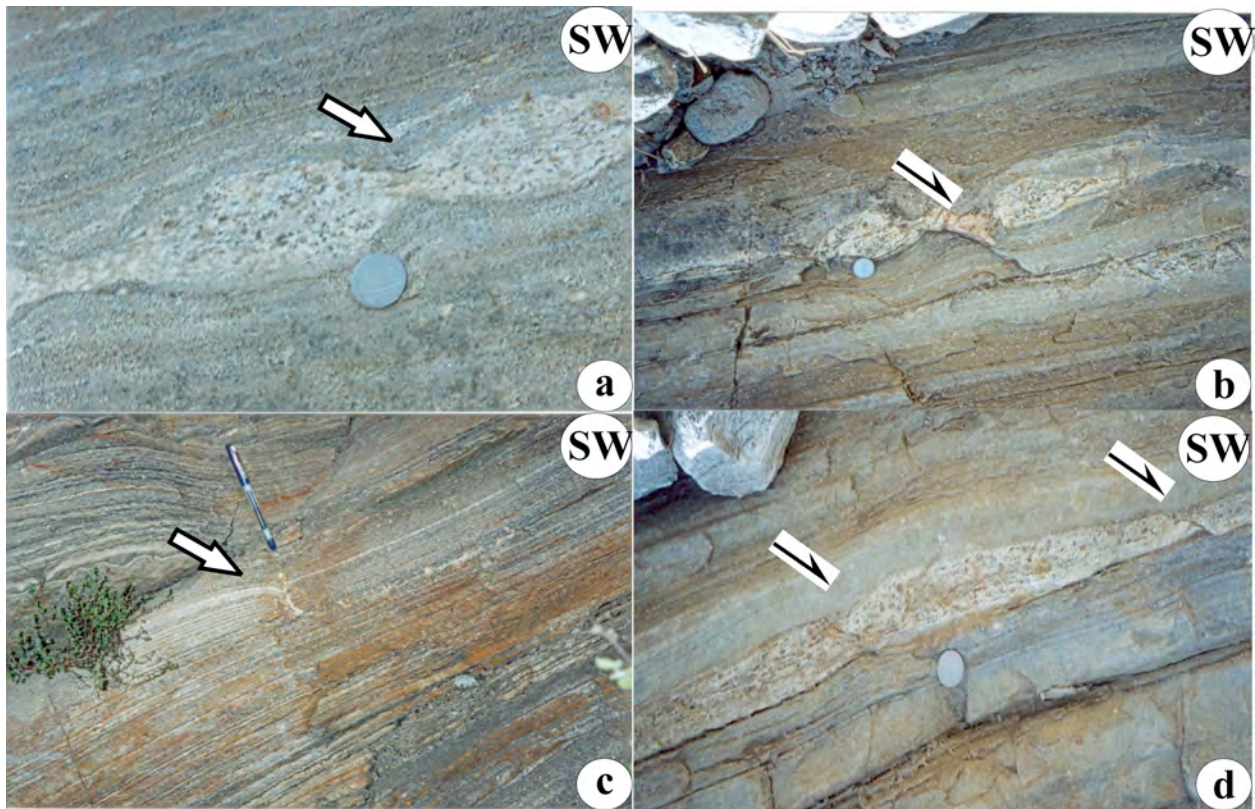


Figure 19a – Pinch and swell structure of calc silicate layer also showing prominent scar folds (arrow). Non-migmatitic rock. Location: 6. 19b – Shear fracture boudin. The shear plane acts as a normal fault. Non-migmatitic rock. Location: 8. 19c – Imperfectly formed boudin with only the development of scar folding (arrow). Non-migmatitic rock. Location: 7. 19d – Shear fracture boudin. The shear plane at one place acts as a normal fault and is lystric in one place. Scar folding prominent. Non-migmatitic rock. Location: 5.

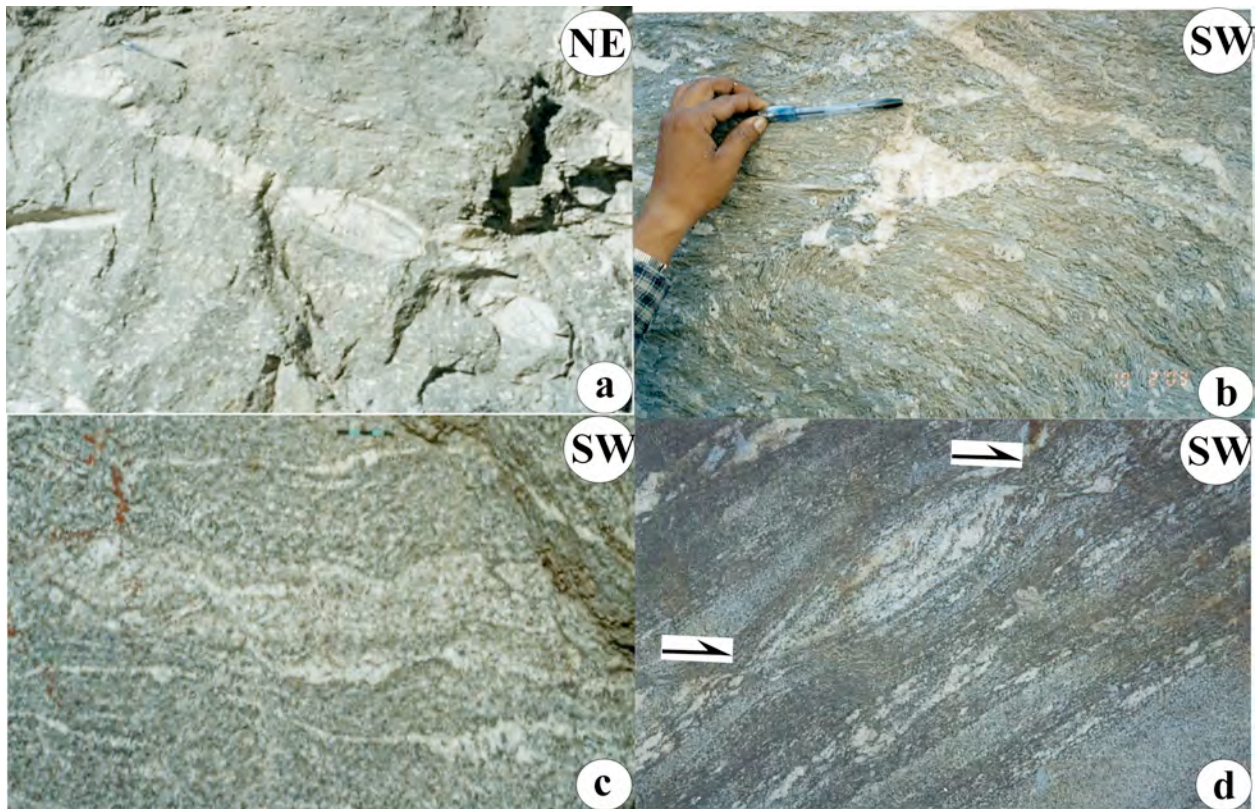


Figure 20a – Lenticular boudin of leucosomes. Migmatite. Location: 14. 20b – Accumulation of quartz rich melt at a boudin neck. Migmatite. Location: 13. 20c – Pinch and swell structure of leucosome. The tectonic force was insufficient to separate leucosomes into pods. Migmatite. Location: 17. 20d – Thick layers of leucosomes and thin layers of melanosomes defining pods that are separated from each other (or boudinaged) by short straight secondary shear planes. Migmatite. Location: 13.



Figure 21 – A thick leucosome layer pinch and swelled. Thin melanosome layers are scar folded. Migmatite. Location: 15.

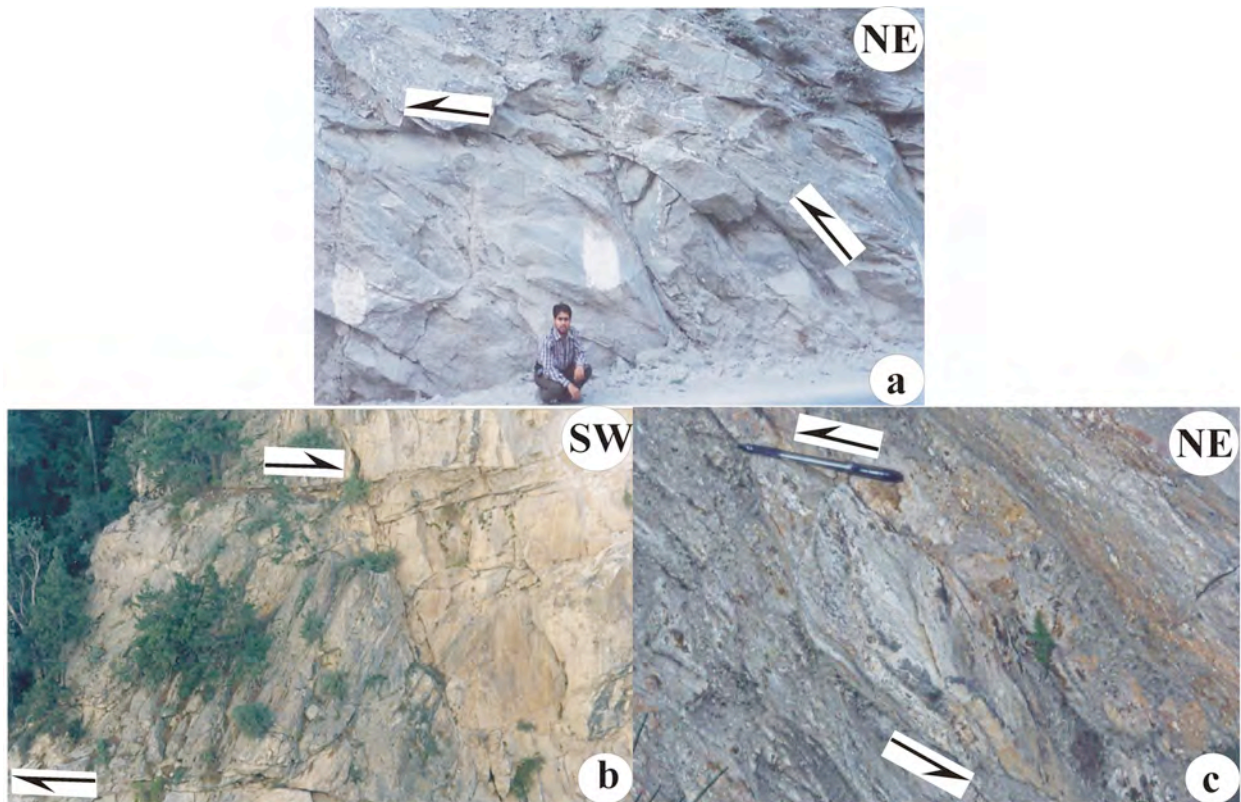


Figure 22a – Duplexes of larger dimension. The P-plane is sigmoid (or zigmoid). The Y-plane is subhorizontal. Migmatite. Location: 9. 22b – Mega-duplexes. Y-planes sub-horizontal. The P-planes are distinct, straight except at their contacts with the Y-planes where they are curved. Migmatite. Location: 12. 22c – Elongated sigmoid bulges of fractured rocks define the P-plane. These planes are confined by sharp straight brittle Y-planes. Non-migmatitic rock. Location: 6.

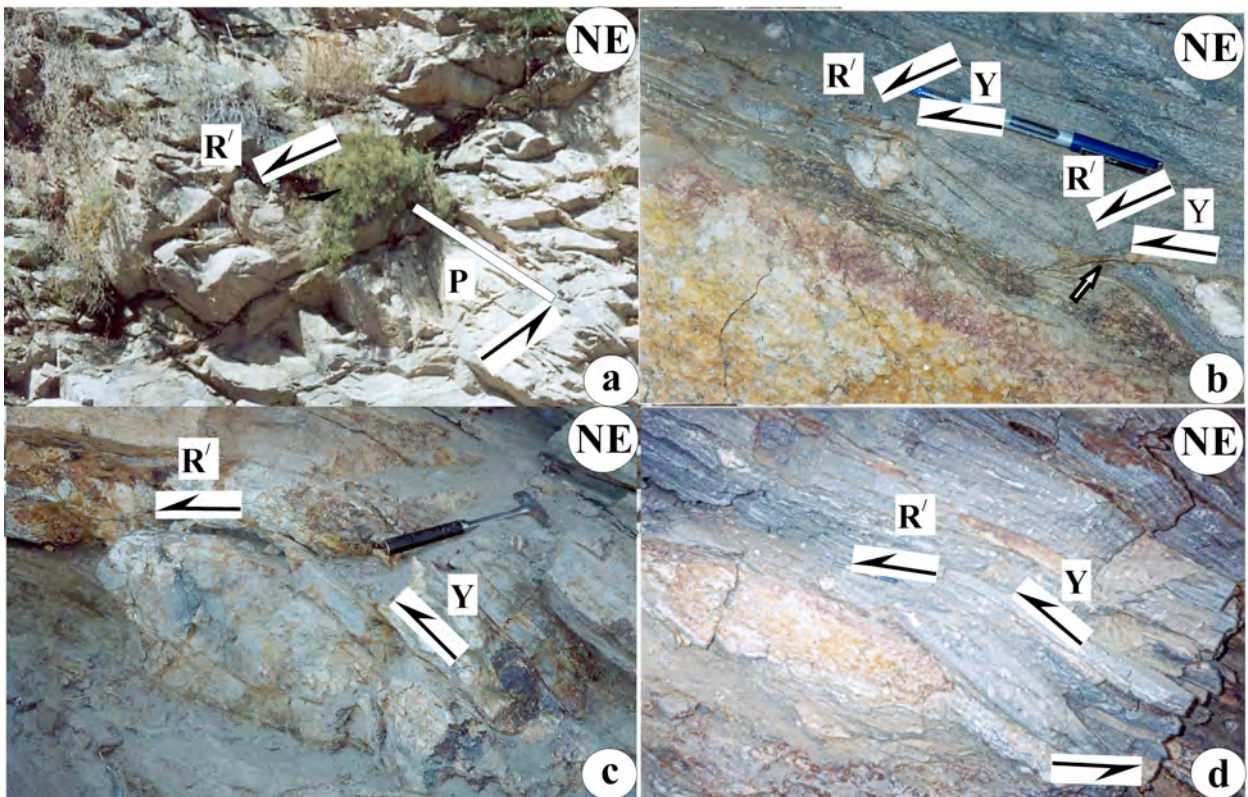


Figure 23a – Synthetic secondary R' -shear plane gave rise to sets of sigmoid bulges of rocks. Migmatite. Location: 14. 23b – Along primary and secondary shear planes, later brittle deformation took place. Arrow points brittle fracture along the C' -shear plane. Migmatite. Location: 20. 23c – A lenticular bulge of rock acts as the P-plane. The Y-plane that bounds it is curved. Location: 11. 23d – The sigmoid (or zigmoid to be more specific) bulge of rock underwent brittle shearing along the ductile shear plane. Short straight secondary R' -plane also prominent. Migmatite. Location: 16.

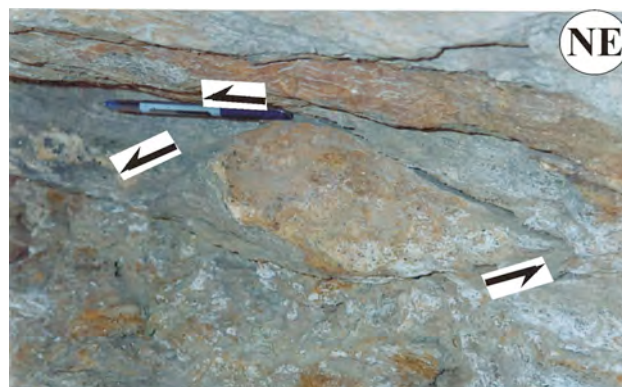


Figure 24 – Sigmoid (or zigmoid- to be more specific) asymmetric bulge of duplex underwent secondary brittle shearing of moderate intensity. Non-migmatitic rock. Location: 4.

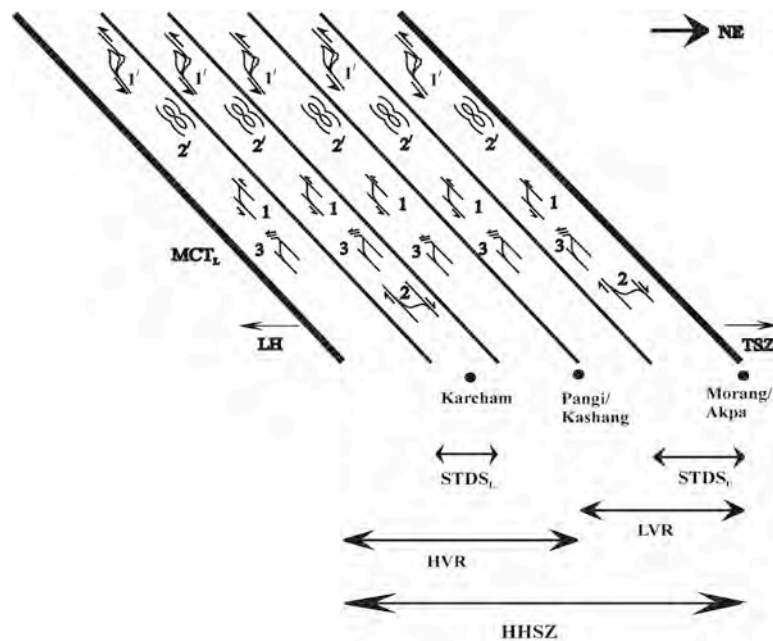


Figure 25 – The first order structural geology of the Sutlej section of the Higher Himalayan Shear Zone (HHSZ) is summarized in a NE-SW cross-section of the shear zone. The HHSZ is bounded by the Lesser Himalaya (LH) in the south and northeasterly dipping Main Central Thrust-Lower (MCT_L), and the Tethyan Sedimentary Zone (TSZ) in the north. Symbols- '1': Top-to-SW compressional ductile shearing. '2': Top-to-NE extensional ductile shearing confined within the $STDS_U$ and the $STDS_L$. '3': Secondary shearing synthetic to '1'. '4': Secondary shearing synthetic to '2'. '1': Top-to-SW brittle shearing. '2': Brittle shearing synthetic to '1'. '3': Boudinaging. Different fabrics were used to decode these deformations but are represented here by their single varieties. 'LVR' stands for the 'low viscosity rocks' and the 'HVR' for the 'high viscosity rocks' that was prevalent during the top-to-NE sense of ductile shearing in the HHSZ. Locations in relation to lithological and structural boundaries are indicated. The Diagram is neither to scale nor angle.

3. CONCLUSIONS

A variety of structures (and textures) are reported from the Sutlej section of the Higher Himalayan Shear Zone (HHSZ) in field and micro-textural studies from the western Indian Himalaya. S-C fabric are documented from both migmatitic and nonmigmatitic rocks. The leucosomes in migmatites are variably aligned along the shear planes indicating that they were emplaced during the ductile deformation process. The S- fabrics vary in curvature but are usually tangential to the C-planes. Leucosomes and melanosomes of various thicknesses define the S- and the C-planes. In micro-scale, single deformed minerals of sigmoid and parallelogram shapes define mineral fish, alternately a number of almost undeformed grains define S-fabrics. Near Karcham, garnet porphyroblasts are extremely stretched parallel to the foliation planes and some are syntectonically grown during the top-to-NE shearing. In micro-scales crenulation cleavages, remnant sedimentary textures and brittle faults were rarely noted. Rather abundant are asymmetric trapezoid-shaped minerals from the HHSZ that connote a top-to-SW sense of brittle shearing. Intrafolial folds of varying style, thick hinges and thin limbs with unequal thickness were observed throughout the shear zone. Extreme shearing led to either sub-parallelism of the axial traces or brittle slip of limbs. The leucosome melt at places are either randomly oriented, or occupy the S- and the C-planes, or locate at the inter-boudin space. Ductile shear sense inside the South-Tibetan Detachment System-Lower ($STDS_L$) and the South-Tibetan Detachment System-Upper ($STDS_U$) is dominantly top-to-NE. Elsewhere in the HHSZ, the ductile shear sense is top-to-SW. Insufficient tectonic force at places left pinch and swell structures.

Elsewhere boudinage seems to be a syn-migmatization process. Isolated and a number of sigmoid thrust blocks define duplexes that consistently reveal a top-to-SW sense of brittle shearing. The brittle deformation was essentially a post-migmatization event.

Acknowledgements

I acknowledge IIT Bombay's flexible 'Seed Grant' (Spons/GS/SM-1/2009) and Chris Talbot's (Uppsala University) mentoring. Ramananda Chakrabarti (Harvard University), Siddhartha Bhattacharyya (Alabama University), Arundhuti Ghatak (Rochester University) and Pritam Nasipuri (Universitetet i Tromsø) constantly updated me with literature. Constructive criticism by the two anonymous reviewers led me to clarify the scientific content of this manuscript.

References

- BELL, T.H. & CUFF, C. (1989) – Dissolution, solution transfer, diffusion versus fluid flow and volume loss during deformation/metamorphism. *Journal of Metamorphic Geology*, 7, 425-447.
- BÈRTHÉ, D., CHOUKROUNE, P. & JEGOUZO, P. (1979) – Orthogneiss, mylonite and non-coaxial deformation of granite: the example of the south Armorican shear zone. *Journal of Structural Geology*, 1, 31-42.
- COTTLE, J.M., JESSUP, M.J., NEWELL, D.L., SEARLE, M.P. & LAW, R.D. (2007) – Structural insights into the early stages of exhumation along an orogen-scale detachment: the South Tibetan Detachment System, Dzaka Chu section, Eastern Himalaya. *Journal of Structural Geology*, 29, 1781-1797.
- GHOSH, S.K. (1993) – *Structural Geology Fundamental and Modern Development*. Pergamon, Oxford.
- GODIN, L., GRUJIC, D., LAW, R.D. & SEARLE, M.P. (2006) – Channel flow, extrusion and exhumation in continental collision zones: an introduction. In: Law RD, Searle MP (eds) *Channel Flow, Extrusion and Exhumation in Continental Collision Zones*. Geol. Soc. London, Spec. Publ., 268, 1-23.
- HIPPERTT, J.F.M. (1993) – 'V' pull-apart microstructures: a new shear sense indicator. *Journal of Structural Geology*, 15, 1393-1403.
- JOHNSON, M.R.W. & HARLEY, S.H. (2003) – Kinematic model for the Main Central thrust in Nepal: Comment and Reply. *Geology*, 31, e40.
- LISTER, L.S. & SNOKE, A.W. (1984) – S-C Mylonites. *Journal of Structural Geology*, 6, 617-638.
- MCCLAY, K.R. & INSLEY, M.W. (1986) – Duplex structures in the lewis thrust sheet, crow's nest pass, rocky mountains, Alberta. Canada. *Journal of Structural Geology*, 8, 911-922.
- MARCHILDON, N. & BROWN, M. (2003) – Spatial distribution of melt-bearing structures in anatexitic rocks from Southern Brittany, France: implications for melt transfer at grain- to orogen-scale. *Tectonophysics*, 364, 215-235.
- MISRA, S., BURLINI, L. & BURG, J.-P. (2009) – Strain localization and melt segregation in deforming metapelites. *Physics of the Earth and Planetary Interiors*, 177, 173-179.

- MUKHERJEE, S. (in press) – Mineral Fish- their morphological classification, usefulness as shear sense indicators and genesis. *International Journal of Earth Sciences*.
- MUKHERJEE, S. (2007) – Geodynamics, deformation and mathematical analysis of metamorphic belts of the NW Himalaya. Unpublished PhD thesis. Indian Institute of Technology Roorkee, 267p.
- MUKHERJEE, S. (2008) – Manifestation of brittle thrusting in micro-scale in terms of micro-duplexes of minerals in the Higher Himalayan Shear Zone, Sutlej & Zaskar section, northwest Indian Himalaya. GeoMod2008. International Geological Modelling Conference. Florence, Italy. 22-24 September. *Bolletino di Geofisica Teorica e Applicata*, 49, 2, 254-257.
- MUKHERJEE, S. & KOYI, H.A. (in press, 1) – Higher Himalayan Shear Zone, Sutlej section: structural geology and extrusion mechanism by various combinations of simple shear, pure shear and channel flow in shifting modes *International Journal of Earth Sciences*.
- MUKHERJEE, S. & KOYI, H.A. (in press, 2) – Higher Himalayan Shear Zone, Zaskar Section- Microstructural Studies & Extrusion Mechanism by a Combination of Simple Shear & Channel Flow. *International Journal of Earth Sciences*.
- MUKHERJEE, S. & KOYI, H.A. (2009) – Flanking Microstructures. *Geological Magazine*, 146, 517-526.
- PASSCHIER, C.W. & TROUW, R.A.J. (2005) – *Microtectonics*. 2nd Ed. Berlin. Springer.
- SINGH, S. (1993) – *Collision Tectonics: Metamorphic and Geochronological Constraints from Parts of Himachal Pradesh, NW-Himalaya*. Unpublished Ph.D. Thesis. University of Roorkee. India. 289 p.
- SRIKANTIA, S.V. & BHARGAVA, O.N. (1998) – *Geology of Himachal Pradesh*. Geological Society of India. Bangalore. 406 p.
- TEN GROTENHUIS, S. M., PASSCHIER, C. W. & BONS, P. D. (2002) – The influence of strain localization on the rotation behaviour of rigid objects in experimental shear zones. *Journal of Structural Geology* 24, 485-499.
- VANNAY, J-C. & GASEMANN, B. (1998) – Inverted metamorphism in the High Himalaya of Himachal Pradesh (NW India): phase equilibria versus thermobarometry. *Schweizerische Mineralogische und Petrographische Mitteilungen* 78, 107-132.
- VANNAY J-C., GASEMANN, B. (2001) – Himalayan inverted metamorphism and syn-convergence extension as a consequence of a general shear extrusion. *Geological Magazine*, 138, 253-276.
- VANNAY, J.-C., GASEMANN, B., RAHN, M., FRANK, W., CARTER, A., BAUDRAZ, V. & COSCA, M. (2004) – Miocene to Holocene exhumation of metamorphic crustal wedge in the NW Himalaya: Evidence for tectonic extrusion coupled to fluvial erosion. *Tectonics*, 23, TC1014, 1-24.
- VANNAY, J-C., SHARP, D.Z., GASEMANN, B. (1999) – Himalayan inverted metamorphism constrained by oxygen thermometry. *Contributions to Mineralogy and Petrology*, 137, 90-101.
- VERNON, R.H. (2004) – *A Practical Guide to Rock Microstructure*. Cambridge.

YIN, A. (2006) – Cenozoic tectonic evolution of the Himalayan orogen as constrained by along strike variation of structural geometry, extrusion history, and foreland sedimentation. *Earth-Science Reviews*, 76, 1-131.

Received: 20 November 2009

Accepted: 10 March 2010

Published: 24 March 2010